# Reduced-order model based on cyclic symmetric properties to tackle nonlinear mistuned cyclic structures

Samuel Quaegebeur*,†, Benjamin Chouvion*, Fabrice Thouverez* and Loïc Berthe†
*Ecole Centrale de Lyon, LTDS UMR 5513, 69130, Ecully, France
†Safran Helicopter Engines, 64511, Bordes, France

*Summary.* This paper deals with cyclic systems, such as for instance turboengines, in the presence of random mistuning and geometrical nonlinearities. A new methodology based on cyclic components is proposed to create a nonlinear reduced-order model. It is applied on a simplified bladed-disk with a cubic nonlinearity for both tuned and mistuned cases. Internal resonances in which several modes of a system exchange energy are recovered. A comparison of the amplification factor due to mistuning between the linear and nonlinear structures is given.

## 1 Introduction

This paper studies the dynamics of cyclic structures such as turboengines. For perfectly tuned linear systems, Valid and Ohayon [1] proved that their model could be written in terms of cyclic components. As underlined in [2, 3], the full system of equations, controlling the dynamics of the structure, can thus be split into multiples much smaller cyclic systems. The modes associated with these cyclic components, also called nodal diameters, form a modal basis of the equations of motion. The thorough review given by Mitra and Epureanu [4] presents the properties of cyclic structures and underlines two ongoing problematics for such systems: the nonlinear and the mistuning effects.
In this paper, geometrical nonlinearities are investigated. As the bypath ratio of turboengines is getting larger, effects due to large deformation are getting more pronounced in recent practical applications. Such nonlinearities couple the different nodal diameters of the system. Consequently the size of the cyclic system becomes equal to the onde of the full system and applying cyclic symmetric properties loses its advantages. However combining the specific cyclic geometry of the structure and nonlinear effects reveals some interesting complex phenomena. These have been widely studied by the scientific community. Vakakis [5] studied the nonlinear characteristics (similar modes, localization, energy transfer) of a simplified tuned cyclic structure and compared his result with experimental ones [6]. Georgiades et al. [7] studied modal interactions occuring in cyclic structures. Sarrouy et al. [8] proposed a methodology to determine the multiple periodic solutions of a tuned cyclic structure. Internal resonances [9], transfer of energy from one mode to another, were investigated in these papers. More recently Grolet et al. [10] and Fontanela et al. [11] studied the phenomenon of dark solitons in cyclic structures. All of these papers solved the full system of equation which is time-consuming. Recently, we propose in [12] a methodology to determine which nodal diameter gets coupled in a tuned cyclic structure. This allows to decrease significantly the size of the problem and to express the nonlinearity in the cyclic domain. With this strategy, employing the cyclic symmetry property gets again more computationally interesting.
Random mistuning corresponds to the presence of small imperfection in the cyclic structure, due to manufacturing tolerances for instance. This theoretically breaks the cyclic symmetry property and the entire system must be solved to capture exactly the whole dynamics. In terms of modal properties, the mistuning leads to a split of frequencies of the degenerated modes as explained in [4, 5]. Methodologies [13, 14] that use cyclic symmetric properties have been developed to reduce the size of the linear system of equations. They assume that the motion of the system is mostly controlled by the tuned modes. In a series of papers, Bladh et al. [15, 16, 17] proposed a new methodology to create a reduced-order model (ROM) in order to perform many simulations for multiple random mistuning patterns. This probability study has provided an amplification factor curve with respect to the level of mistuning. This amplification factor is defined as the ratio of the maximal displacement of the mistuned structure over the tuned one. Such analysis is time-consuming, even for linear problems, but the concept of amplification factor is extremely interesting for engines manufacturers. Studies [18] have shown that intentional mistuning patterns (large and controlled difference between the sectors) reduce the impact of random mistuning on the response amplitude and thus allow a better prediction of the system dynamics.
In this paper, both random mistuning and geometrical nonlinearity are considered. The objective is to present a new methodology to create non-linear ROMs that can be used to predict amplification factor of nonlinear mistuned structures. Section 2 presents how mistuning and nonlinearities can be taken into account in a cyclic formulation. Section 3 details the new ROM methodology that is based on these cyclic components. The simplified bladed-disk (blisk) used as test-case will be presented in Section 4. Finally, a probability approach will then be conducted in Section 5 to determine the amplification factor for the linear and nonlinear blisk systems.

## 2 Cyclic symmetry formulation

This section first recalls the cyclic symmetric properties of a linear system before introducing nonlinearities and mistuning.

### 2.1 Linear cyclic symmetric systems

Let consider a cyclic structure composed of $N$ identical sectors (tuned system), such as the one illustrated in Figure 1. The dynamics of the entire structure is described with the equation:

$$\mathbf{M}\ddot{\mathbf{u}} + \mathbf{C}\dot{\mathbf{u}} + \mathbf{K}\mathbf{u} = \mathbf{f}_{\text{ext}}, \tag{1}$$

where $\mathbf{M}$, $\mathbf{C}$ and $\mathbf{K}$ represent the mass, damping and stiffness matrices. The vectors $\mathbf{u}$ and $\mathbf{f}_{\text{ext}}$ denote the displacement and the external forces associated with the entire structure. As detailed in [3, 12] the cyclic symmetry property only requires to model a single sector (whose mass, damping and stiffness matrices will be noted $\mathbf{M}_0$, $\mathbf{C}_0$ and $\mathbf{K}_0$). Applying the spectral Fourier matrix $\mathbf{F}$ (normalized by a factor $\sqrt{N}$) and the matrix $(\mathbf{B}_k)_{k\in[\![0,K]\!]}$ (where $K = \frac{N}{2}$ if $N$ is even and $\frac{N-1}{2}$ otherwise) which relates to a phase change function of the nodal diameter considered between the left and right boundaries of a sector, one obtains the following decoupled equation of motion in the cyclic domain for each nodal diameter $k$,

$$\tilde{\mathbf{M}}_k\ddot{\tilde{\mathbf{u}}}_k + \tilde{\mathbf{C}}_k\dot{\tilde{\mathbf{u}}}_k + \tilde{\mathbf{K}}_k\tilde{\mathbf{u}}_k = \tilde{\mathbf{f}}_k, \tag{2}$$

where $\tilde{\mathbf{M}}_k = \bar{\mathbf{B}}_k^T\bar{\mathbf{F}}\mathbf{M}_0\mathbf{F}\mathbf{B}_k$ and similarly for the damping and stiffness matrices. The operators $.^T$ and $\bar{.}$ denote respectively the tranpose of a vector or matrix and the complex conjugate. The vectors $\tilde{\mathbf{u}}_k$ and $\tilde{\mathbf{f}}_k$ represent the cyclic component of the displacement and the external forces associated with the nodal diameter $k$. The initial problem (Equation (1)) contains $N \times N_{\text{dof}}$ unknowns (with $N_{\text{dof}}$ the number of degrees of freedom of one sector). It is transformed into $N$ independent problems with $N_{\text{dof}}$ unknowns each (corresponding to Equation (2) applied $\forall k \in [\![0, K]\!]$).

In turboengines application, one stage of blisk usually gets excited by another stage. This creates an excitation force with specific properties: in most cases the excitation either follows a traveling or a standing wave pattern. The associated wave number of the excitation force will be noted $h_{ex}$ [19]. As a consequence, Equation (2) needs only to be solved for this specific nodal diameter $h_{ex}$ as the remaining nodal diameters are not excited and therefore do not respond.

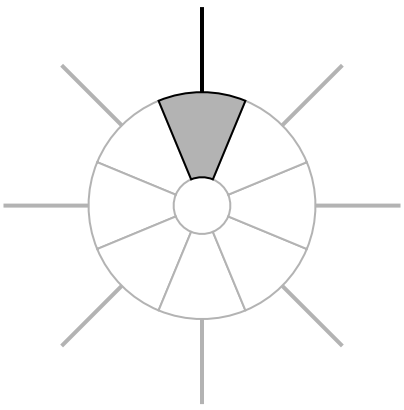

Figure 1: General cyclic structure. The cyclic symmetry property requires to model only a single sector such as the one illustrated in grey color.

### 2.2 Nonlinear cyclic symmetric systems

In the presence of internal nonlinearities (the cyclic boundaries are assumed to be free of nonlinear forces), the system (2) gets coupled from the nonlinear terms and needs to be solved for all $k$ simultaneously. The equation of motion in the cyclic domain becomes:

$$\tilde{\mathbf{M}}_k\ddot{\tilde{\mathbf{u}}}_k + \tilde{\mathbf{C}}_k\dot{\tilde{\mathbf{u}}}_k + \tilde{\mathbf{K}}_k\tilde{\mathbf{u}}_k + \tilde{\mathbf{f}}_{\text{nl},k}\left(\tilde{\mathbf{u}}\right) = \tilde{\mathbf{f}}_k, \qquad \forall k \in [\![0, K]\!], \tag{3}$$

where $\tilde{\mathbf{f}}_{\text{nl},k}\left(\tilde{\mathbf{u}}\right)$ are the cyclic nonlinear forces for the $k-$th nodal diameter. Those are function of the displacement written here in terms of cyclic components such that $\tilde{\mathbf{u}} = \left[\tilde{\mathbf{u}}_0^T, ..., \tilde{\mathbf{u}}_K^T\right]^T$. The components $\tilde{\mathbf{u}}_k$ for the degenerated diameters ($k \in [\![1, K-1]\!]$ if $N$ is even and $k \in [\![1, K]\!]$ if $N$ is odd) are complex values. The nonlinear terms couple a priori all nodal diameters. Therefore the system (3) has the same size as (1).

In some of our recent work [12], we showed how to identify which nodal diameter get coupled for a given excitation when the structure exhibits polynomial nonlinearities. Applying this methodology reduces the system (3) to the following

$$\tilde{\mathbf{M}}_k\ddot{\tilde{\mathbf{u}}}_k+\tilde{\mathbf{C}}_k\dot{\tilde{\mathbf{u}}}_k+\tilde{\mathbf{K}}_k\tilde{\mathbf{u}}_k+\tilde{\mathbf{f}}_{\mathrm{nl},k}\left(\tilde{\mathbf{u}}\right)=\tilde{\mathbf{f}_k},\qquad\forall k\in\left(k_m\right),\tag{4}$$

where $k_m$ is a reduced set of the interacting nodal diameters found by the methodology explained in [12]. In practice the nonlinear term $\tilde{\mathbf{f}}_{\mathrm{nl},k}$ can be either obtained by calculating the nonlinear forces in the physical domain (function of the displacement and using Fourier transforms back and forth) or by computing them directly in the cyclic domain (see the method proposed in [12]).

### 2.3 Nonlinear mistuned cyclic symmetric systems

Only random mistuning (small variations between sectors) is considered in this work. Stiffness variations are assumed but the method can be easily extended for mass or damping mistuning. Consider the cyclic system illustrated in Figure 1 and assume that each sector shows a slight variation in its stiffness matrix such that, for a sector $j$, its stiffness is defined with

$$\mathbf{K}_j=\mathbf{K}_0+\Delta\mathbf{K}_j,\tag{5}$$

where $\Delta\mathbf{K}_j$ denotes the mistuned part of sector $j$. In order to get the general equation of motion in the cyclic domain, one applies the same cyclic symmetric procedure (the same projections) as explained above despite the fact that the sectors are not necessarily all identical. The system of equations becomes

$$\tilde{\mathbf{M}}_k\ddot{\tilde{\mathbf{u}}}_k+\tilde{\mathbf{C}}_k\dot{\tilde{\mathbf{u}}}_k+\tilde{\mathbf{K}}_k\tilde{\mathbf{u}}_k+\Delta\tilde{\mathbf{K}}_{k,a}\tilde{\mathbf{u}}+\Delta\tilde{\mathbf{K}}_{k,b}\bar{\tilde{\mathbf{u}}}+\tilde{\mathbf{f}}_{\mathrm{nl},k}\left(\tilde{\mathbf{u}}\right)=\tilde{\mathbf{f}}_{\mathrm{ext},k},\qquad\forall k\in[\![0,K]\!],\tag{6}$$

When applying the Fourier matrix, the physical mistuned matrix gets split into $\Delta\tilde{\mathbf{K}}_a$ and $\Delta\tilde{\mathbf{K}}_b$. They are respectively multiplied by $\tilde{\mathbf{u}}$ and its complex conjugate.. In (6), $\Delta\tilde{\mathbf{K}}_{k,a}$ and $\Delta\tilde{\mathbf{K}}_{k,b}$ represent these mistuned parts impacting the $k-$th nodal diameter. The construction of these matrices follows standard linear algebra from the cyclic symmetric properties and are not detailed here for brevity. As highlightened in (6), the mistuning effect also creates coupling between the cyclic components (the whole $\tilde{\mathbf{u}}$ vector is present) and thus the system must be solved for all nodal diameters simultaneously.
For better readibility, the different equations (6) for all $k$ are concatenated using block diagonal matrices and it gives

$$\tilde{\mathbf{M}}\ddot{\tilde{\mathbf{u}}}+\tilde{\mathbf{C}}\dot{\tilde{\mathbf{u}}}+\tilde{\mathbf{K}}\tilde{\mathbf{u}}+\Delta\tilde{\mathbf{K}}_a\tilde{\mathbf{u}}+\Delta\tilde{\mathbf{K}}_b\bar{\tilde{\mathbf{u}}}+\tilde{\mathbf{f}}_{\mathrm{nl}}\left(\tilde{\mathbf{u}}\right)=\tilde{\mathbf{f}}_{\mathrm{ext}}\tag{7}$$

The purpose of the new methodology presented in this study is to compute a nonlinear reduced-order model (ROM) of system (7).

## 3 Methodology to create a nonlinear ROM

The following methodology is based on the theory of normal nonlinear mode (NNM) developed by Rosenberg [21] and the synthesis procedure of Szemplinsky [22].

### 3.1 Evaluation of the NNMs

The first step of the proposed ROM creation is to compute the NNMs associated with the $k-$th cyclic component of the underlying perfect cyclic symmetric system. They are defined as the solutions of the following autonomous and conservative system associated with (4) in which only the nodal diameter $k$ is taken into account in the nonlinear term (the system is thus decoupled),

$$\tilde{\mathbf{M}}_k\ddot{\tilde{\mathbf{u}}}_k+\tilde{\mathbf{K}}_k\tilde{\mathbf{u}}_k+\tilde{\mathbf{f}}_{\mathrm{nl},k}\left(\tilde{\mathbf{u}}_k\right)=\mathbf{0}.\tag{8}$$

The NNMs are computed with the Harmonic Balance Method (HBM) with a pseudo arc-length procedure [20]. The solution of (8) is supposed periodic of fundamental frequency $\omega$ and sought as

$$\tilde{\mathbf{u}}_k=\sum_{n=-N_h}^{N_h}\tilde{\mathbf{c}}_{k,n}\mathrm{e}^{\mathrm{i}n\omega t}.\tag{9}$$

where $N_h$ is the maximum number of harmonics retained and $\tilde{\mathbf{c}}_{k,n}$ are the harmonics coefficients of the $k-$nodal diameter. For a degenerated diameter, each harmonic coefficient is independent as $\tilde{\mathbf{u}}_k$ is a complex vector; however for non-degenerated diameters, one has $\tilde{\mathbf{c}}_{n,k}=\bar{\tilde{\mathbf{c}}}_{n,-k}$ and thus a real vector is obtained. Substituting (9) in (8) and projecting the system on the exponential basis with the scalar product,

$$\langle f,g\rangle=\frac{1}{T}\int_0^T f\left(t\right)\bar{g}\left(t\right)\mathrm{d}t,\tag{10}$$

one retrieves the HBM system of equations to solve with $\tilde{\mathbf{c}}_{k,n}$ and $\omega$ as unknowns. The nonlinear forces are evaluated with the Alternating Frequency Time (AFT) procedure [23]. In practice, for an intialization on mode $i$, we only retrieve for each nodal diameter the harmonics coefficients $-1$ and 1: $\tilde{\mathbf{c}}_{i,k,\pm1}$. These are then normalized by a control coordinate and are used to form the vector denoted later $\boldsymbol{\phi}^{\mathrm{nl}}_{i,\pm1}$, which provides the shape of the displacement for all DOFs parametrized by the control coordinate.

### 3.2 Synthesis procedure

The second step is to build a nonlinear reduction basis. The solution of (7) is sought after in the form of (11) for each nodal diameter (index $k$). The cyclic displacement of each of these nodal diameters is defined with multiple nonlinear modes (index $i$ up to $I$) whose calculation is explained in Section 3.1, supplemented by multiple linear modes (index $m$ up to $M$).

$$\begin{aligned}\tilde{\mathbf{u}}_k \;=\; & \sum_{i=1}^{I}\left[\boldsymbol{\phi}^{\mathrm{nl}}_{i,1}\left(\left|\boldsymbol{\alpha}^{\mathrm{nl}}_{i,n>0}\right|\right)\left(\sum_{n=1}^{N_h}\alpha^{\mathrm{nl}}_{i,n}\mathrm{e}^{\mathrm{i}\,n\omega t}\right)+\boldsymbol{\phi}^{\mathrm{nl}}_{i,-1}\left(\left|\boldsymbol{\alpha}^{\mathrm{nl}}_{i,n<0}\right|\right)\left(\sum_{n=-1}^{-N_h}\alpha^{\mathrm{nl}}_{i,n}\mathrm{e}^{\mathrm{i}\,n\omega t}\right)\right] \\ & +\sum_{m=1}^{M}\left[\boldsymbol{\phi}^{\mathrm{lin}}_{m}\left(\alpha^{\mathrm{lin}}_{m,1}\mathrm{e}^{\mathrm{i}\omega t}+\alpha^{\mathrm{lin}}_{m,-1}\mathrm{e}^{-\mathrm{i}\omega t}\right)\right] \qquad\qquad \forall k\in[\![0,K]\!].\end{aligned} \tag{11}$$

The generalized coordinates associated with the NNMs are approximated with a Fourier expansion (of order $N_h$) whose coefficients are $\alpha^{\mathrm{nl}}_{i,n}$. As explained in [21], $\boldsymbol{\phi}^{\mathrm{nl}}_{i,\pm1}\left(\left|\boldsymbol{\alpha}^{\mathrm{nl}}_{i}\right|\right)$ depends on the amplitude of the generalized coordinates and is thus evaluated via an interpolation process at every solver iteration. Linear modes can also be added to the synthesis procedure if necessary and those are represented by mode shapes $\boldsymbol{\phi}^{\mathrm{lin}}_m$ and generalized coordinates $\alpha^{\mathrm{lin}}_{m,1}$ and $\alpha^{\mathrm{lin}}_{m,-1}$. Equation (11) is the synthesis associated with a degenerated nodal diameter: each NNM is split into two parts (the positive and negative harmonic coefficients) to respect the eigenvalue multiplicity. For a non-degenerated diameter, the cyclic component is only controlled with its positive harmonic (its negative counterpart is its complex conjugate). Mathematically the reduction (11) can also be written as

$$\tilde{\mathbf{u}}_k=\sum_{n=-N_h}^{N_h}\tilde{\mathbf{c}}_{k,n}\mathrm{e}^{\mathrm{i}n\omega t},\qquad\forall k\in[\![0,K]\!], \tag{12}$$

where the harmonic coefficients are sought after as

$$\begin{pmatrix}\tilde{\mathbf{c}}_{-N_h}\\ \vdots\\ \tilde{\mathbf{c}}_{n}\\ \vdots\\ \tilde{\mathbf{c}}_{N_h}\end{pmatrix}=\underbrace{\left(\boldsymbol{\phi}^{\mathrm{nl}}\left(\left|\boldsymbol{\alpha}^{\mathrm{nl}}\right|\right)\quad\boldsymbol{\phi}^{\mathrm{lin}}\right)}_{\boldsymbol{\Phi}}\underbrace{\begin{pmatrix}\boldsymbol{\alpha}^{\mathrm{nl}}\\ \boldsymbol{\alpha}^{\mathrm{lin}}_{1}\\ \boldsymbol{\alpha}^{\mathrm{lin}}_{-1}\end{pmatrix}}_{\boldsymbol{\alpha}}, \tag{13}$$

where $\tilde{\mathbf{c}}_n=[\tilde{\mathbf{c}}_{0,n},...,\tilde{\mathbf{c}}_{K,n}]^T$ gathers the $n-$th harmonic coefficients of all nodal diameters and $\boldsymbol{\alpha}^{\mathrm{nl}}$ is the concatenation of $\left(\boldsymbol{\alpha}^{\mathrm{nl}}_{i,n}\right)_{(i,n)\in[\![1,I]\!]\times[\![-N_h,Nh]\!]}$. Similarly, the unknowns $\boldsymbol{\alpha}^{\mathrm{lin}}_{\pm1}$ contains the generalized coordinates for the different linear modes. The matrix $\boldsymbol{\Phi}$ is created by combining appropriately the different basis: the NNMs and the linear modes. The solution (12) is substituted in (7) and the system is then projected in the exponential basis (see Equation (10)). This gives:

$$\begin{pmatrix}\tilde{\mathbf{Z}}_{-N_h}&\cdots&0\\ \vdots&\ddots&\vdots\\ 0&\cdots&\tilde{\mathbf{Z}}_{N_h}\end{pmatrix}\begin{pmatrix}\tilde{\mathbf{c}}_{-N_h}\\ \vdots\\ \tilde{\mathbf{c}}_{N_h}\end{pmatrix}+\begin{pmatrix}0&\cdots&\Delta\tilde{\mathbf{K}}_b\\ \vdots&\iddots&\vdots\\ \Delta\tilde{\mathbf{K}}_b&\cdots&0\end{pmatrix}\begin{pmatrix}\bar{\tilde{\mathbf{c}}}_{-Nh}\\ \vdots\\ \bar{\tilde{\mathbf{c}}}_{N_h}\end{pmatrix}+\begin{pmatrix}\tilde{\mathbf{c}}_{\mathbf{f}_{\mathrm{nl},-N_h}}\\ \vdots\\ \tilde{\mathbf{c}}_{\mathbf{f}_{\mathrm{nl},N_h}}\end{pmatrix}=\begin{pmatrix}\tilde{\mathbf{c}}_{\mathbf{f}_{\mathrm{ext},-N_h}}\\ \vdots\\ \tilde{\mathbf{c}}_{\mathbf{f}_{\mathrm{ext},N_h}}\end{pmatrix} \tag{14}$$

where $\tilde{\mathbf{Z}}_n=(\mathrm{i}n\omega)\tilde{\mathbf{M}}+(\mathrm{i}n\omega)\tilde{\mathbf{C}}+\tilde{\mathbf{K}}+\Delta\tilde{\mathbf{K}}_a$ is the dynamical rigidity matrix associated with the harmonic $n\in[\![-N_h,N_h]\!]$. The vectors $\tilde{\mathbf{c}}_{\mathbf{f}_{\mathrm{nl},n}}$ and $\tilde{\mathbf{c}}_{\mathbf{f}_{\mathrm{ext},n}}$ gather the $n-$th harmonic coefficients of all nodal diameters for the nonlinear and external forces. The nonlinear forces are evaluated with the same procedure as the one explained in Section 3.1. The harmonic coefficients in (14) are then substituted by (13). Finally, the last stage of the ROM creation is premultiplying this equation by $\boldsymbol{\Phi}^T$,

$$\left(\bar{\boldsymbol{\Phi}}^T\tilde{\mathbf{Z}}\boldsymbol{\Phi}\right)\boldsymbol{\alpha}+\left(\bar{\boldsymbol{\Phi}}^T\left(\mathbf{J}_{1+2N_h}\otimes\Delta\tilde{\mathbf{K}}_b\right)\bar{\boldsymbol{\Phi}}\right)\bar{\boldsymbol{\alpha}}+\bar{\boldsymbol{\Phi}}^T\tilde{\mathbf{c}}_{\mathbf{f}_{\mathrm{nl}}}=\bar{\boldsymbol{\Phi}}^T\tilde{\mathbf{c}}_{\mathbf{f}_{\mathrm{ext}}}, \tag{15}$$

where $\tilde{\mathbf{Z}}$ is a block diagonal matrix containing $\left(\tilde{\mathbf{Z}}_n\right)_{n\in[\![-N_h,N_h]\!]}$. The vectors $\boldsymbol{\alpha}$, $\tilde{\mathbf{c}}_{f_{\mathrm{nl}}}$ and $\tilde{\mathbf{c}}_{f_{\mathrm{ext}}}$ are vertically concatenated. The matrix $\mathbf{J}_{1+2N_h}$ is the exchange matrix ($\mathbf{J}_{1+2N_h,i,j}=\delta_{2N_h+2-i,j}$).
To couple the different modes, the nonlinear forces (term $\tilde{\mathbf{c}}_{\mathbf{f}_{\mathrm{nl}}}$) are evaluated with the AFT procedure while solving (15).

Even though the notation suggests that the same expansion is performed for each nodal diameter, the new methodology can be adjusted and each nodal diameter written with different modal basis and harmonic expansion.
This formulation is different from the synthesis proposed by Krack et al. [24] for the following reasons: the reduced Equation (15) uses cyclic components, a multi-harmonic expansion and a reevaluation of the nonlinear forces (once with the NNM evaluation and once with the synthesis stage).
In practice, the unknowns of system (15), $\boldsymbol{\alpha}$, are solved with a Newton-Raphson solver. For better efficiency, the semi-analytical jacobian of this system is provided to the solver. The work of Joannin et al. [25] provides insights on how to compute the jacobian in a similar problem.

### 3.3 Choice of nodal diameters and modes

The methodology proposed is efficient if the user chooses wisely the NNMs to compute, the linear modes and the HBM expansion order. As explained in Section 2, turboengines are usually excited by a specific excitation force with a given wave number $h_{ex}$. Moreover only random mistuning is accounted in this paper which induces an assumed slight variation around the tuned response of the system.
As a consequence, only NNMs of the nodal diameters that interact in the tuned system (see [12]) are evaluated. In the case of a mistuned structure, corrections are made possible by taking into account the linear modes of the remaining nodal diameters.
The selection of which modes to compute depends on the probability of the appearance of internal resonances and thus on the spectral repartition of the natural frequencies of the system.

## 4 Application for a tuned and a mistuned blisks

The purpose of this Section is to validate the methodology explained in Section 3. The reference solution used for validation is the HBM employed on the full system with $N_h = 3$ harmonics. Comparison of computation time between the reference solution and the ROM procedure is provided in Section 4.4.

### 4.1 Simplified model and ROM creation

The proposed methodology is tested on a simplified blisk composed of $N = 24$ sectors, one of which is illustrated in Figure 2. A cubic nonlinearity is applied at the tip of the blade to model symmetric large displacement. This test case was already used in [12] to study a perfectly tuned structure. The mass, damping and stiffness values can be found in Tables 1 and 2 of the aforementioned article. Figure 3 represents the natural frequencies of the underlying linear tuned system. In the remaining of the article, an external force with $h_{ex} = 3$ is applied and is set to excite the first mode of the nodal diameter 3 of the system. Based on [12], we know that the third and ninth nodal diameters will be coupled. Moreover, Figure 3 allows to see that the first and third modes of the nodal diameter 3 are almost commensurable, and similarly for the first and second modes of the ninth nodal diameter. As a consequence 1:3 internal resonances may occur. The NNMs computed will therefore be those associated with these 4 natural frequencies (depicted by red circles in Figure 3). In the rest of this section, the reduction basis used is composed of these 4 NNMs, expanded with the HBM up to $N_h = 3$, associated with more or less linear modes depending on the situation.

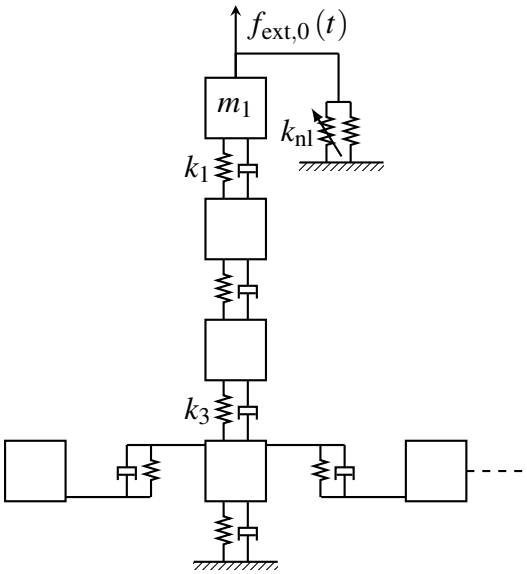


Figure 2: Description of the simplified blisk.

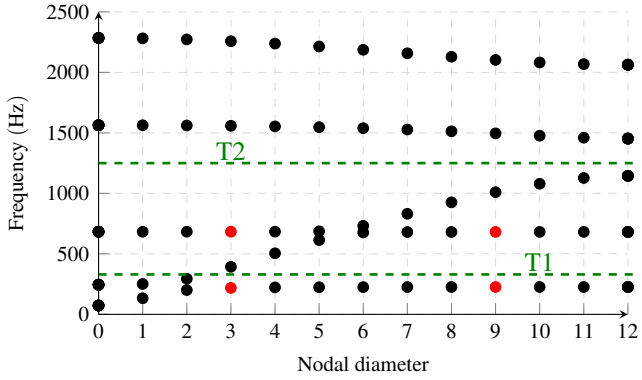


Figure 3: Natural frequencies for each nodal diameter.

The tuned system is first studied in Section 4.2. Section 4.3 focuses on mistuning and a random mistuning pattern is introduced on top of the spring stiffness values $k_1$ and $k_3$, see Figure 2. The new stiffnesses are defined as

$$k_{m,i} = k_i(1+\varepsilon\xi_i), \qquad i \in \{1,3\} \tag{16}$$

where $k_{m,i}$ is the mistuned stiffness value used instead of $k_i$ ($i = 1$ ou 3). The parameters $\varepsilon$ and $\xi_i$ are the mistuning parameters: $\varepsilon$ controls the level of mistuning ($\varepsilon \in [0,1]$) and $\xi_i$ is a random value taken from an uniform law in $[-0.1, 0.1]$. Table 1 provides the random mistuning pattern used in this section.

| Sectors | S1 | S2 | S3 | S4 | S5 | S6 | S7 | S8 |
|---|---|---|---|---|---|---|---|---|
| $\xi_1$ (in%) | 0.0094 | −8.8 | −9.2 | 0.43 | 6.4 | 4.4 | 3.2 | 9.5 |
| $\xi_3$ (in%) | −0.583 | 3.6 | −8.6 | −8 | 6.4 | −7 | 0.37 | 3 |
| | S9 | S10 | S11 | S12 | S13 | S14 | S15 | S16 |
| | 6 | −1.4 | −8.3 | −6.5 | 6.6 | −8.8 | 0.54 | 3.1 |
| | −0.92 | 6.5 | −7.3 | −2.2 | 6.1 | −2 | −1.7 | 2.6 |
| | S17 | S18 | S19 | S20 | S21 | S22 | S23 | S24 |
| | −4.2 | −9.7 | −6.7 | −2.6 | −0.21 | −9 | −8.9 | −4.6 |
| | −1.4 | 9.7 | −7.9 | −6 | −3.2 | 8.4 | 4.8 | −1.5 |

Table 1: Numerical values used for $\xi$.

For each simulation, a bifurcation analysis [26] and branch switching algorithms [27] are performed. Solving (15) provides the generalized coordinates which can then be employed to recover the displacement of the entire structure. In the following section, the results illustrated are the displacement amplitude of the mass $m_1$ for the third and ninth nodal diameters. Those are noted respectively $\tilde{u}_3$ and $\tilde{u}_9$.

### 4.2 Results for the tuned structure

First the ROM procedure is validated for the tuned model. The external force is applied on mass $m_1$, and is defined as:

$$\tilde{f}_{\text{ext},3} = 25\left(e^{-i\omega t} + e^{i\omega t}\right). \tag{17}$$

This high amplitude force was chosen to exhibit multiple nonlinear phenomena for the tuned case and thus to verify the accuracy of the ROM for these complex situations.

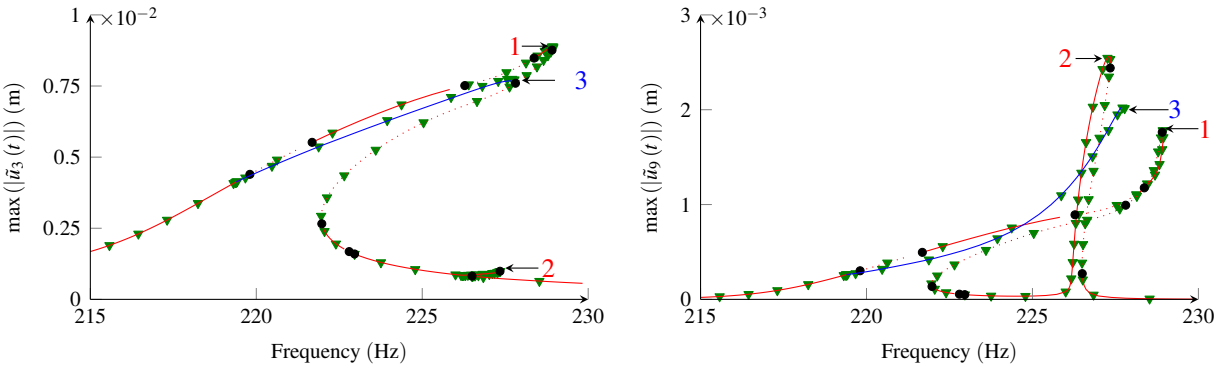


Figure 4: Frequency forced response for the tuned system. (▼): reference solution; (—): ROM solution for the stable main branch; (····): ROM solution for the unstable main branch; (—): ROM solution for the bifurcated branch; (●): bifurcation points.

The results obtained with the ROM procedure and the reference solution are provided in Figure 4. Two branches are represented: the main branch of solution and a bifurcated branch initiated from a symmetry-breaking bifurcation (only the stable part of this branch is represented in Figure 4). The ROM solution perfectly matches the reference solution with a huge computational time saving as detailed in Table 2. Multiple internal resonances are obtained in Figure 4. They are highlightened by arrows and number and the harmonics coefficients of the response at these points are represented in Figure 5. For the peak numbered 1, on the main branch, $\tilde{u}_3$ mainly responds with its first harmonic (see Figure 5a); however $\tilde{u}_9$ responds both on its first and third harmonics. It shows that a 1:1 and 1:3 internal resonances have taken place. For the peak numbered 2, still located on the main branch, the amplitude of $\tilde{u}_9$ is higher than $\tilde{u}_3$ (see Figure 5b) and is mainly due to

its first harmonic. An 1:1 internal resonance is occuring. Notice that for both of these peaks, the solution has a standing wave form similar to the external force (because $\tilde{c}_{k,n} = -\tilde{c}_{k,-n}$). For the peak numbered 3 located on the bifurcated branch, the solution has a forward traveling wave shape (because $\tilde{c}_{k,n<0} \neq 0$ and $\tilde{c}_{k,n>0} = 0$). Moreover Figure 5c shows a 1:3 internal resonance.

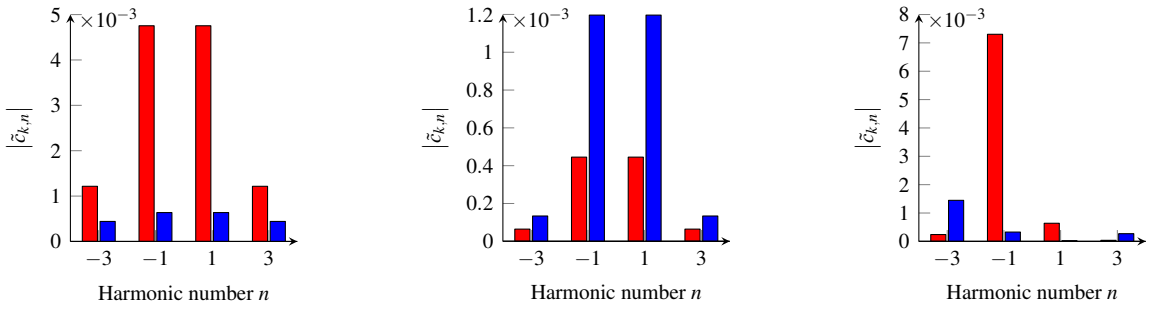


(a) Peak 1 (main branch). (b) Peak 2 (main branch). (c) Peak 3 (bifurcated branch).

Figure 5: Amplitude of the harmonics coefficients of the response at the three peaks mentioned in Figure 4. (—): $\tilde{c}_{3,n}$; (—): $\tilde{c}_{9,n}$. The second harmonic is not represented as it is exactly equal to 0.

The same model was used in [12] with a different reduction procedure and similar results were obtained. Overall, this example has shown that the proposed ROM is perfectly able to recover complex phenomena such as internal resonances and branch switching for a tuned system.

### 4.3 Results for the mistuned structure

The random mistuning pattern given in Table 1 is now introduced in the system. Three values of $\varepsilon$ are studied: 0.01, 0.1 and 1, corresponding respectively to a deviation of 0.1%, 1% and 10% between the tuned and mistuned systems. A traveling wave excitation is applied on $m_1$ such that

$$\tilde{f}_{\text{ext},3} = 2.5\text{e}^{-\text{i}\omega t}. \tag{18}$$

This force is 10 times smaller than the standing wave force used for the tuned case and its amplitude is more typical of turboengines applications.

For $\varepsilon = 0.01$ and $\varepsilon = 0.1$, the nonlinear basis is supplemented with all the linear modes below the threshold 1 of Figure 3 (represented by the dashed green line T1) that are used to take into account the other nodal diameters. For $\varepsilon = 1$, the system is largely mistuned (10% deviation) and the first three modes of each nodal diameter are included in the reduction basis (represented by the dashed green line T2 in Figure 3). For this system, all nodal diameters are coupled and respond; however only the third and ninth nodal diameters will be represented as they control the main dynamics. The stability of the response was not studied as the main purpose of the article is to validate the accuracy of the ROM with respect to the reference solution.

Figure 6 represents the forced response for the three values of $\varepsilon$. For these different configurations, no bifurcated branch was obtained. As $\varepsilon$ increases, the amplitude of $\tilde{u}_3$ and $\tilde{u}_9$ decreases. The energy initially contained in these two nodal diameters is gradually transfered to the rest of the nodal diameters due to the mistuning effect. Moreover, we can observe the appearance of multiple linear resonances for the third and ninth nodal diameters. This is expected as frequency splitting occurs [28]. The new methodology perfectly matches the result of the reference solution.

In mistuned systems, detecting internal resonances is an arduous task as all nodal diameters are expected to respond. Figure 7 represents the harmonic coefficients of $\tilde{u}_3$ and $\tilde{u}_9$ for the peaks represented in Figure 6. For peak 1 of Figure 6a ($\varepsilon = 0.01$), the solution shows a traveling shape and the third harmonic of $\tilde{u}_9$ is dominant. It gives evidence to a 1:3 internal resonance (see Figures 7a). Similar results are obtained for peak 3 of Figure 6b ($\varepsilon = 0.1$) as shown in Figures 7b. The peaks 2 and 4 for the $\varepsilon = 0.01$ and $\varepsilon = 0.1$ are associated with a standing wave solution as depicted in Figures 7d and 7e for instance. For both peaks of Figure 6c ($\varepsilon = 1$), the solution has a standing wave shape and only the first harmonic responds for $\tilde{u}_3$ and $\tilde{u}_9$.

Obtaining a standing wave solution, even though the excitation is defined with a traveling form, was expected for mistuned system [28]. However Figure 7 presents an interesting trend: as $\varepsilon$ increases, the internal resonances progressively disappear. Studying succesively Figure 7a, 7b and 7c (increase of $\varepsilon$), one can observe that the amplitude of the third harmonic of $\tilde{u}_9$ diminishes in aid of the first harmonic. As a consequence, it is expected that large mistuning would remove internal resonances. In order to make a definitive statement, further studies should be conducted but these are beyond the scope of this paper

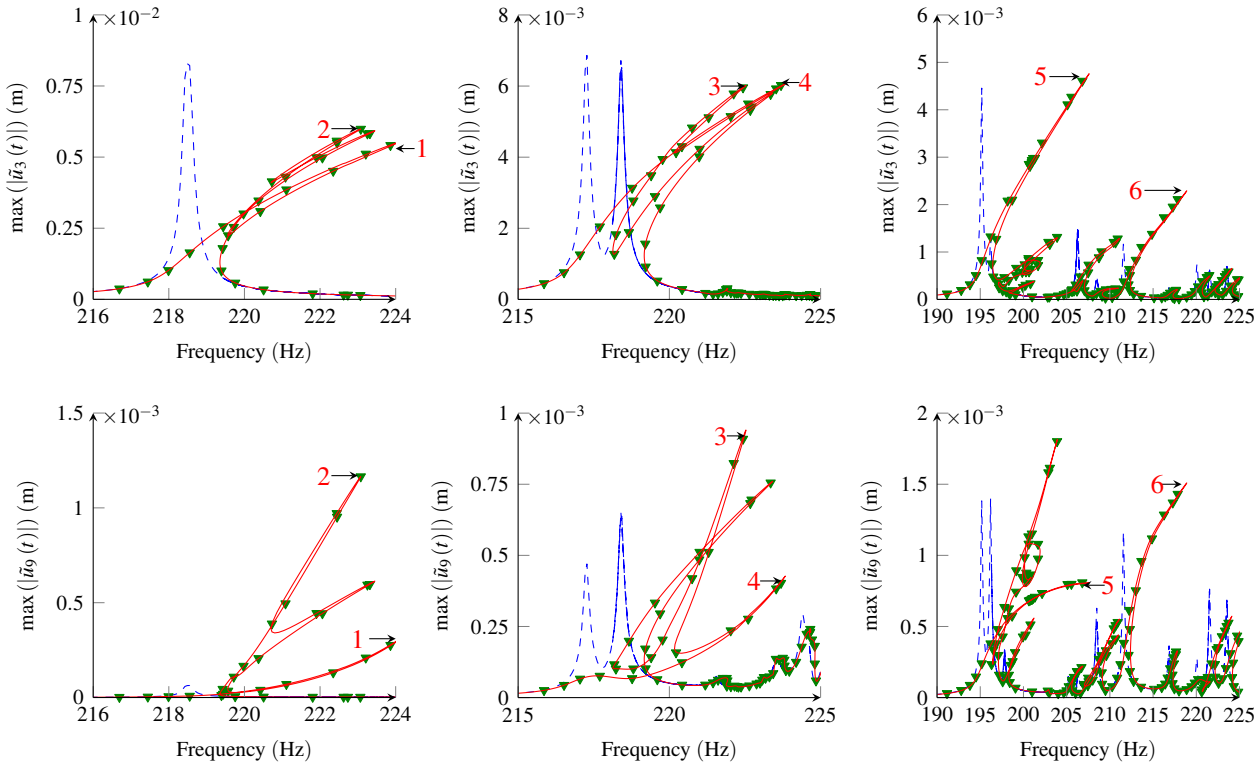


(a) $\varepsilon = 0.01$. (b) $\varepsilon = 0.1$. (c) $\varepsilon = 1$

Figure 6: Frequency response function for different levels of mistuning. (- - ): linear response; the rest of the legend matches the one of Figure 4.

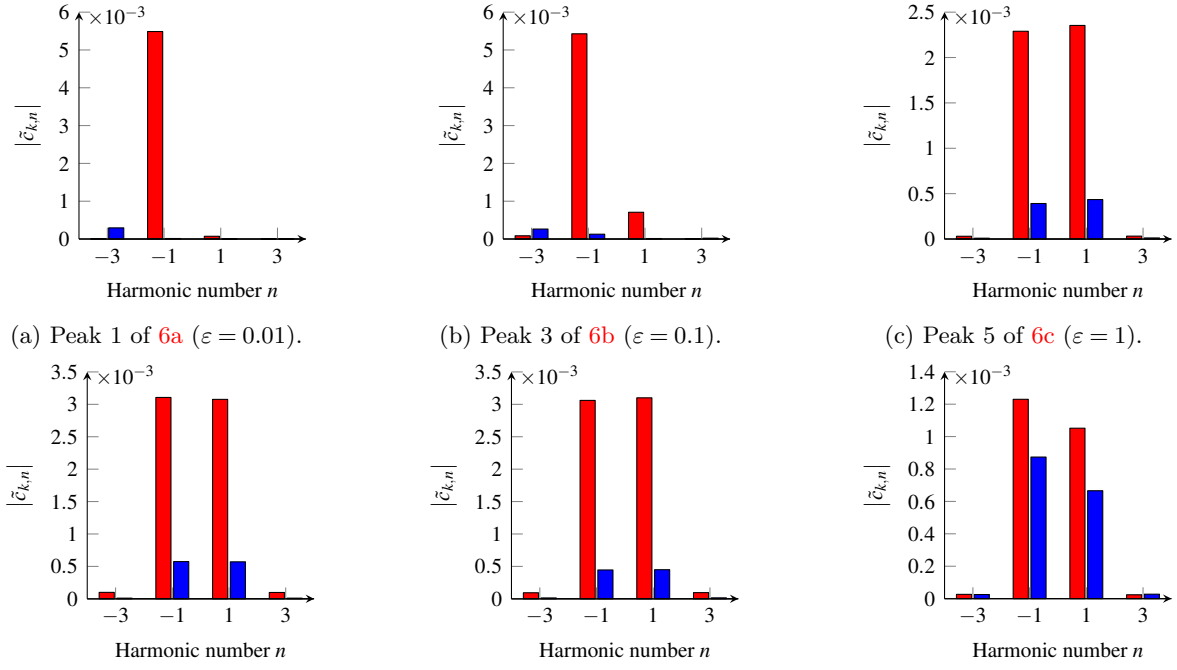


(a) Peak 1 of 6a ($\varepsilon = 0.01$). (b) Peak 3 of 6b ($\varepsilon = 0.1$). (c) Peak 5 of 6c ($\varepsilon = 1$).

(d) Peak 2 of 6a ($\varepsilon = 0.01$). (e) Peak 4 of 6b ($\varepsilon = 0.1$). (f) peak 6 of 6c ($\varepsilon = 1$).

Figure 7: Harmonics content for the response on the six peaks of Figure 6. The legend matches the one of Figure 5.

### 4.4 Computation time comparison

For both tuned and mistuned systems, the proposed ROM has shown great accuracy and enables to recover complex nonlinear phenomena. Table 2 compares the computation time between the ROM and the reference solutions.

| Test case | Method | Number of unknowns | Computation time (min) |
|---|---|---|---|
| Tuned system | Reference | 720 | 24 |
| | ROM | 48 | 3 |
| Mistuned system ($\varepsilon = 0.01$) | Reference | 720 | 59 |
| | ROM | 108 | 24 |
| Mistuned system ($\varepsilon = 0.1$) | Reference | 720 | 145 |
| | ROM | 108 | 43 |
| Mistuned system ($\varepsilon = 1$) | Reference | 720 | 202 |
| | ROM | 186 | 81 |

Table 2: Computation time for the different test cases and methodologies. The simulations were run on a standard computer with Intel Core i7 2.30GHz 8Go.

The computation time of the new methodology is greatly reduced compared to the reference solution (2 to 8 times faster). The computation time of the NNMs is not taken into account in Table 2 as it is negligible (below 20 s and needs to be computed only once for all simulations).

## 5 Amplification factor

When considering mistuned systems, turboengineers are used to study the maximal amplitude of the (physical) displacement obtained over all sectors. The amplification factor (AF) is defined as the ratio between this maximum amplitude and the amplitude of the (single) peak obtained in a perfectly tuned system. This is illustrated in Figure 8 for the linear case. We propose a similar definition in the presence of nonlinearity, see Figure 9. Both of these Figures are obtained on the test case of Figure 2 with a 2.5 N traveling wave excitation and $h_{ex} = 3$. The mistuning pattern is the one presented in Table 1 with $\varepsilon = 0.1$.

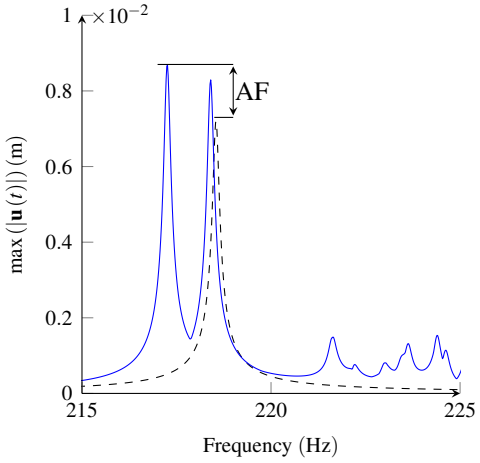


Figure 8: Tuned (- -) and mistuned (—) linear frequency forced responses.

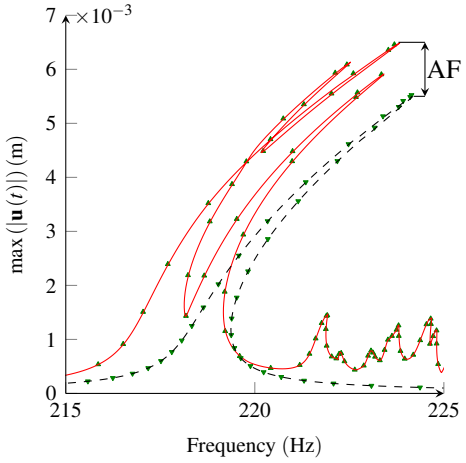


Figure 9: Tuned (- -) (respectively (▼)) and mistuned (—) (respectively (▲)) nonlinear frequency forced responses obtained with the ROM (respectively the reference solution).

The amplification factor relates to the amplification of the response due to the mistuning. In practice, one must generate a large number of random mistuning patterns to determine the overall behaviour of the AF. Extended studies have performed such tasks [17, 29] for linear systems. For instance, to determine accurately the 95$^{\text{th}}$ AF threshold (corresponding to 95% of mistuned blisks below this AF), one way is to launch a Monte Carlo simulation with a large number of samples. The simulation consists in randomly picking a large number of mistuning patterns (for a given law), and sweep the excitation frequency for each of them to determine the associated maximal amplitude. If one wants to reach a given accuracy, then the larger the AF-threshold, the

more simulations must be run. These calculations are time-consuming but it was shown, for instance in [17], that the distribution of the AF law was a three-parameter Weibull law, and this allows to reduce greatly the number of simulations needed. In the following, we have used a Weibull law reconstructed with only 50 simulations.
We have run these simulations for a 2.5 N traveling force and $h_{ex} = 3$. The mistuning definition follows Equation (16) with $\varepsilon = 1$ and $\xi$ is taken within an uniform law with 15 different standard deviations (from 1% to 15% with a step of 1%). Figure 10a represents the AF with respect to the standard deviation for the linear system. Figure 10b provides the same information for the nonlinear system. For both of these Figures, the $95^{\text{th}}$, $50^{\text{th}}$ and $5^{\text{th}}$ percentiles (percentage of systems below the threshold) are represented. The maximum AF is obtained for $\varepsilon_{\max} \approx 3\%$ for the linear system and $\varepsilon_{\max} \approx 9\%$ for the nonlinear one. The value of the maximum AF is close to 1.9 for the linear system and 1.8 for the nonlinear one. Beyond this value of $\varepsilon_{\max}$, the AF decreases. This behaviour has already been observed, in [29] for instance. The ROM solution matches well the reference solution with a significant computational time saving: the trend is correctly captured and errors are below 7% for a high level of mistuning.
Notice that the results were obtained with a specific excitation force. While Figure 10a remains valid for other levels of excitation (at $h_{ex}$ fixed), the nonlinear results of Figure 10b are expected to vary. For a complete map of the influence of the mistuning, one must run these computations for all values of $h_{ex}$ as well as for different force amplitudes.

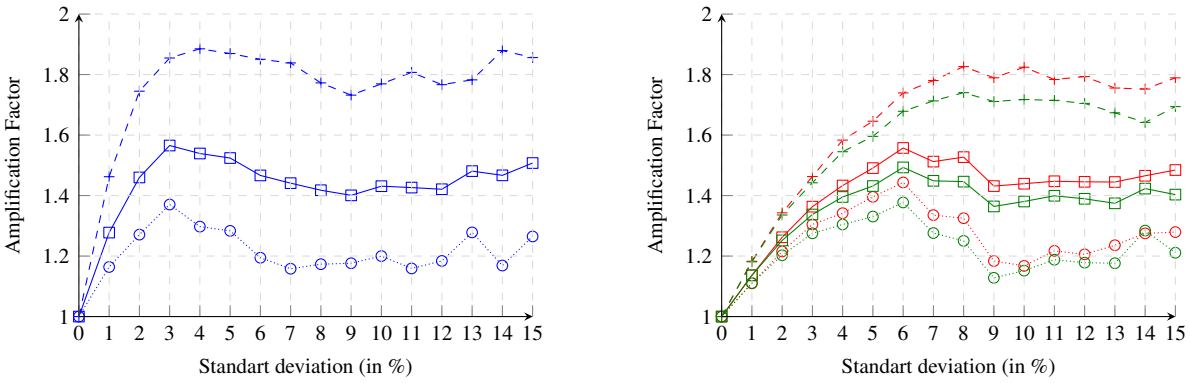


(a) Linear Solution.

(b) Nonlinear solution for the ROM/reference procedures.

Figure 10: Amplification factor with respect to the deviation of the random mistuned pattern. (-+ ):$95^{\text{th}}$ percentile; (-⊟-): $50^{\text{th}}$ percentile; (··o··): $5^{\text{th}}$ percentile. The blue, red and green colors denote respectively the linear case, the ROM and the reference solutions for the nonlinear case.

## 6 Conclusion

This paper presented a new reduced-order model methodology based on the computation of cyclic normal nonlinear modes. It is able to handle randomly mistuned cyclic structures while exhibiting complex nonlinear behaviour such as internal resonances. The method has been validated for a simplified blisk and has shown great accuracy while reducing significantly the computation time.
A probabilist study was conducted to study the impact of both the nonlinearity and the mistuning on the amplification factor of the system. For both linear and nonlinear systems, mistuning may lead to an amplification of 90% in the response. This maximum is however reached for different values of standard deviation. For both systems a plateau is reached after a relatively large value of standard deviation.
This new methodology is expected to be applicable and efficient for finite-element models of engineered structures. It thus offers probabilist opportunities which, at this date, could not be achieved. However, applying the same procedure to intentional mistuned structures (large discrepancies between the blades) is expected to be less efficient because the system is no longer close to its tuned counterpart.

## Acknowledgements

The authors would like to acknowledge the financial support of Safran Helicopter Engines.

## References

[1] Valid R. and Ohayon R. 1985 Théorie et calcul statique et dynamique des structures à symétries cycliques. *La Recherche aérospatiale*

[2] MacNeal, R. H. 1973 NASTRAN cyclic symmetry capability.

[3] Thomas, D. L. 1979 Dynamics of rotationally periodic structures *International Journal for Numerical Methods in Engineering*

[4] Mitra, M. and Epureanu, B.I. 2019 Dynamic Modeling and Projection-Based Reduction Methods for Bladed Disks With Nonlinear Frictional and Intermittent Contact Interfaces *ASME, Applied Mechanics Reviews*

[5] Vakakis, A. F. 1992 Dynamics of a nonlinear periodic structure with cyclic symmetry *Acta Mechanica*

[6] Tobias, S. A. and Arnold, R. N. 1957 The Influence of Dynamical Imperfection on the Vibration of Rotating Disks *Proceedings of the Institution of Mechanical Engineers*

[7] Georgiades F. and Peeters M. and Kerschen G. and Golinval J. C. and Ruzzene M. 2009 Modal Analysis of a Nonlinear Periodic Structure with Cyclic Symmetry. *AIAA Journal*

[8] Sarrouy, E. and Grolet, A. and Thouverez, F. 2011 Global and bifurcation analysis of a structure with cyclic symmetry *International Journal of Non-Linear Mechanics*

[9] Nayfeh, Ali H. and Mook, Dean T. 2008 Nonlinear Oscillations *John Wiley & Sons*

[10] Tobias, S. and Grolet, A. and Hoffmann, N. and Thouverez, F. and Schwingshackl, C. 2016 Travelling and standing envelope solitons in discrete non-linear cyclic structures *Mechanical Systems and Signal Processing*

[11] Fontanela, F. and Grolet, A. and Salles, L. and Chabchoub, A. and Hoffmann, N. 2018 Dark solitons, modulation instability and breathers in a chain of weakly nonlinear oscillators with cyclic symmetry *Journal of Sound and Vibration*

[12] Quaegebeur S. and Chouvion B. and Thouverez F. et al. 2020 Energy transfer between nodal diameters of cyclic symmetric structures exhibiting polynomial nonlinearities: Cyclic condition and analysis. *Mechanical Systems and Signal Processing*

[13] Yang, M.-T. and Griffin, J. H. 1999 A Reduced Order Model of Mistuning Using a Subset of Nominal System Modes *American Society of Mechanical Engineers*

[14] Feiner, D. M. and Griffin, J. H. 2002 A Fundamental Model of Mistuning for a Single Family of Modes *American Society of Mechanical Engineers*

[15] Bladh, R. and Castanier, M. P. and Pierre, C. 2001 Component-Mode-Based Reduced Order Modeling Techniques for Mistuned Bladed Disks Part I: Theoretical Models *American Society of Mechanical Engineers*

[16] Bladh, R. and Castanier, M. P. and Pierre, C. 2001 Component-Mode-Based Reduced Order Modeling Techniques for Mistuned Bladed Disks Part II: Applications *Journal of Engineering for Gas Turbines and Power*

[17] Bladh, R. and Castanier, M. P. and Pierre, C. 2002 Dynamic Response Predictions for a Mistuned Industrial Turbomachinery Rotor Using Reduced-Order Modeling *Journal of Engineering for Gas Turbines and Power*

[18] Castanier, M.P. and Pierre, C. 2002 Using Intentional Mistuning in the Design of Turbomachinery Rotors *AIAA Journal*

[19] Grolet, A. and Thouverez, F. 2012 Free and forced vibration analysis of a nonlinear system with cyclic symmetry: Application to a simplified model *Journal of Sound and Vibration*

[20] Kerschen, G. and Peeters, M. and Golinval, J. C. and Vakakis, A. F. 2009 Nonlinear normal modes, Part I: A useful framework for the structural dynamicist *Mechanical Systems and Signal Processing*

[21] Rosenberg, R. M. 1962 The Normal Modes of Nonlinear n-Degree-of-Freedom Systems *Journal of Applied Mechanics*

[22] Szemplińska-Stupnicka, W. 1979 The modified single mode method in the investigations of the resonant vibrations of non-linear systems *Journal of Sound and Vibration*

[23] Cameron, T. M. and Griffin, J. H. 1989 An Alternating Frequency/Time Domain Method for Calculating the Steady-State Response of Nonlinear Dynamic Systems *Journal of Applied Mechanics*

[24] Krack M.,and Panning-von Scheidt L. and Wallaschek J. 2013 A method for nonlinear modal analysis and synthesis: Application to harmonically forced and self-excited mechanical systems. *Journal of Sound and Vibration*

[25] Joannin, C. and Chouvion, B. and Thouverez, F. and Ousty, JP and Mbaye, M. 2017 A nonlinear component mode synthesis method for the computation of steady-state vibrations in non-conservative systems *Mechanical Systems and Signal Processing*

[26] Seydel, R. 2010 Practical Bifurcation and Stability Analysis *Springer-Verlag*

[27] Xie, L. and Baguet, S. and Prabel, B. and Dufour, R 2017 Bifurcation tracking by Harmonic Balance Method for performance tuning of nonlinear dynamical systems *Mechanical Systems and Signal Processing*

[28] Joannin, C. and Chouvion, B. and Thouverez, F. and Mbaye, M. and Ousty, J.-P. 2015 Nonlinear Modal Analysis of Mistuned Periodic Structures Subjected to Dry Friction *Journal of Engineering for Gas Turbines and Power*

[29] Castanier, M.P. and Pierre, C. 2006 Modeling and analysis of mistuned bladed disk vibration: Status and emerging directions *AIAA Journal*